Internal Stresses, Normal Modes, and Nonaffinity in Three-Dimensional Biopolymer Networks

E. M. Huisman and T. C. Lubensky

Phys. Rev. Lett. **106**, 088301 — Published 25 February 2011

DOI: 10.1103/PhysRevLett.106.088301

Internal stresses, normal modes and non-affinity in three-dimensional biopolymer networks

E.M. Huisman[1], T.C. Lubensky[2]

[1]Universiteit Leiden, Instituut-Lorentz, Postbus 9506, NL-2300 RA Leiden, The Netherlands
[2]Department of Physics and Astronomy, University of Pennsylvania, Philadelphia, PA 19104

We numerically investigate deformations and normal modes of three-dimensional networks of semi-flexible biopolymers as a function of average crosslink coordination number z and relative strength of bending and stretching energies. Our networks consist of filaments that in equilibrium are in a state of internal stress, and they exhibit shear rigidity below the Maxwell isostatic point. In contrast to two-dimensional networks, ours exhibit nonaffine bending-dominated response in all rigid states, including those approaching the maximum of $z = 4$ as long as bending energies are smaller than stretching ones.

PACS numbers: 63.50.-x,87.16.Ka,83.60.Bc

Networks of semi-flexible bio-polymers (NSFP) [1–4] are important for determining and controlling the mechanical properties of eukaryotic cells. Understanding their properties, in particular the relation between mechanical response and network architecture, has been a major goal of biophysics research. NSFPs consist of long filaments of average length L linked two at a time by crosslinks so that each is connected to at most four others [5–8]. The crosslinks we consider, which we will refer to as nodes, allow free rotations of filaments relative to each other. They divide the filaments into a series of segments, of average length l_c, that give rise to a central force between nodes determined by the force-extension curve of a semi-flexible polymer. In addition, bending forces favor parallel alignment of contiguous segments on the same filament meeting at a common node. The mechanical properties of NSFPs depend on their connectivity, parameterized by the average coordination number z of their nodes or by the ratio L/l_c, on their interaction parameters, and on their architecture.

Networks of semi-flexible polymers have much in common with those that occur in network glasses [9–11]. They are both continuous random networks [12]; they both have nodes with maximum coordination number 4; and they are both stabilized below the central-force rigidity threshold by bending forces, between all bonds in the latter but only between segments in the same filament in the former. Careful mode counting and study of the mode structure of network glasses [9–11] and other random systems such as hard spheres near the jamming transition [13–15] have provided fundamental insight into the physics of these systems. They have also been used in the study of two dimensional NSFPs [16, 17]. In this article, we undertake a similar study of simulated three-dimensional NSFPs [18] as a function of their connectivity and interaction parameters, and we analyze the zero-frequency shear modulus and the mode structure as a function of these parameters.

A system of nodes and links in d dimensions has a trivial set of zero-frequency modes of rigid translations and rotations. If the system has additional internal zero-frequency "floppy" modes [10], it is mechanically unstable, though it is often stable with respect to macroscopic stress. As Maxwell [20] first showed, in an unstressed system a global estimate of the number of floppy modes N_0 can be calculated by subtracting the number of constraints N_c from the number of degrees of freedom, $N_0 = dN - N_c$ (neglecting the sub-extensive trivial zero modes), where N is the number of nodes. In the following we consider the forces as constraints. We define N_k as the number of nodes on filament k and N_F as the number of filaments, and in our simulations we explicitly remove all disconnected clusters and all filaments with $N_k = 0$ and $N_k = 1$. Each node is shared by exactly two filaments, and $N = \frac{1}{2}\sum N_k$. In our system, each of the $N_k - 1$ segments on a filament provides one constraint for a total of $N_s = \sum_{k>1}(N_k - 1) = 2N - N_F$ compressional constraints. Because segments on a single filament that meet at a common node are not parallel in our system, each of the $N_k - 2$ nodes on filament k not connected to a dangling end contributes a single constraint for a total of $N_b = \sum_{k>1}(N_k - 2) = 2N - 2N_F$ bending constraints. Thus, $N_0 = dN - N_s - N_b = 3N_F - (4-d)N$. We define the average coordination $z \equiv 2N_s/N$. Then $N_F/N = 2 - (z/2)$, $N_0 = N[2 + d - (3/2)z]$, and the critical coordination number below which floppy modes first appears is $z_c = (2/3)(2+d)$. In $2d$ $z_c = 8/3$, and in $3d$, $z_c = 10/3$, a value that, as expected, is greater than the value $12/5$ in $3d$ network glasses [10]. It is common practice to characterize NSFPs by L/l_c rather than by z. In our case, dangling ends each contribute an average of $l_c/2$ to the length of a segment. Thus L/l_c is equal to the number of nodes per polymer, $\sum_k N_k/N_F = 2N/N_F = (1 - \frac{1}{4}z)^{-1}$, and $(L/l_c)_c = 6$ in $3d$.

We do not represent all monomers explicitly but rather integrate out all degrees of freedom of the polymers between nodes. Since we consider the small-strain behavior of the filaments, we use the linear approximation to the non-linear force-extension curve of semi-flexible polymers. Our Hamiltonian is thus a sum over all segment free energies and over all bending energies of pairs of segments that are connected along a filament, resulting in:

$$\frac{E}{k_B T} = \sum_i \frac{l_p^2}{l_{c,i}^4}(r_i - r_{0,i})^2 + \beta \sum_{i,j} \frac{l_p}{l_{c,i} + l_{c,j}} \Theta_{i,j}^2, \qquad (1)$$

where l_p is the persistence length of the filaments, l_{c_i}, r_i and $r_{0,i}$ are respectively the polymer length, the end-to-end length and the equilibrium end-to-end length of segment i, and $\Theta_{i,j}$

is the angle between segment i and j.

We construct our networks via a Monte Carlo relaxation process. We start with a random, isotropic network that can be considered as a single filament that crosses itself one thousand times [18]. After a large number of Monte Carlo moves that alter the topology of the network, we cut segments of this filament, until we obtain an average filament length L. We assign a polymer length l_c^s to each segment such that the equilibrium end-to-end length of each segment is equal to the actual distance between the nodes they connect. After generation, the network is in equilibrium, but the filaments are slightly bent - $\Theta_{i,j} \neq 0$ - and, as a result, there are internal stresses in the system. For all networks, during generation we keep $l_c = \sum_s l_c^s/N_s$, l_p and β fixed, such that $l_p/l_c \approx 16$ and $\beta = 1.0$. l_p is a measure for the relative stiffness of bending versus stretching. In order to isolate the effects of bending and stretching without altering the network structure and contour lengths, we vary β. We could, however, vary l_p at constant l_c to produce the same effect. Letting $l_p \rightarrow \beta^{-1} l_p^0$, where l_p^0 is the value of l_p at $\beta = 1$ reproduces Eq. (1) with energy measured in unit of $\beta^2 k_B T$. Thus with $l_p^0/l_c = 16$, $\beta = 10.0$ coincides with $l_p/l_c = 1.6$ and $\beta = 0.1$ with $l_p/l_c = 160$. In addition we vary L - and thus the average number of nodes per filament L/l_c - by changing the number of segments we cut. Finally we focus on an experimentally relevant parameter space, with networks with on average 4, 5, 6, 8, 12 and 20 nodes per filament or equivalently with coordination number $z = 3.0$, 3.2, 3.33, 3.5, 3.66 and 3.8. In real-life networks, typical ratios between l_p and l_c coincide with values of β ranging from 0.05 (e.g. cortical actin networks [19]) to 10 (e.g. fibrin networks [5]); here we take values of β ranging from 0.0001 to 10. All data shown are averages over nine network realizations.

We calculate the dynamical matrix from the harmonic expansion of the energy about its force-free equilibrium state and use commercially available routines to find the eigenvalues and eigenmodes of the system, neglecting any damping effects arising in particular from interactions with a surrounding fluid. Fig. 1 graphically represents one localized and one delocalized eigenmode.

To investigate the Maxwell mode counting in our networks, we remove the internal stresses by subtracting the zero strain angle, $\Theta_{i,j,0}$, between two segments from the actual angle $\Theta_{i,j}$ in our Hamiltonian. We then count the number of zero modes by calculating the dimension of the null space of the dynamical matrix, and we verify the relation $N_0 = N[5 - \frac{3}{2}z]$. We verify the stretching relation, $N_s = \sum(N_k - 1)$, by explicitly counting the number of finite-frequency modes for networks with $\beta = 0$, and thus no bending constraints. We also verify that $N_b = \sum_k (N_k - 2)$ by varying the number of nodes with non-zero bending modulus β. When internal stresses are turned back on, the floppy modes are tightened, and there are only finite-frequency modes for all z (≥ 3.0) and all $\beta > 0$. Also the lengthening of a single segment in the unstressed samples generates stress in a finite fraction of the segments and elevates floppy modes to finite frequency a full 10% below the Maxwell threshold. This is comparable to the rigid

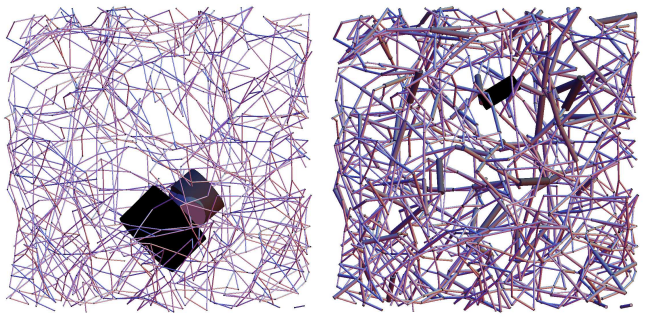

FIG. 1: Graphical representations of two eigenmodes of one our networks, left: ($\omega = 27$, $P^{-1} = 0.51$) and right: ($\omega = 1.4$, $P^{-1} = 0.0029$), where ω is the eigenfrequency and P^{-1} is the inverse participation ratio (see the discussion of Fig. 3). All filaments in the networks are shown. The thick and dark beams indicate large deformations.

"stressed" state of network glasses, that exists for z just below the Maxwell threshold of 2.4 [11].

We calculate the relaxed shear modulus G for networks with and without internal stresses and for a range of z and β by deforming the network by a small shear increment and minimizing the elastic energy after each shear increment. Fig. 2 summarizes our results. For all values of β, $G(z)$ is a monotonic increasing function of z, reaching its lowest but non-zero value at $z = 3.0$, the smallest values in our simulations. As shown by the dotted curve in the inset of Fig. 2, in the unstressed networks, G is zero to within the accuracy of our simulations for $z < z_c$ and develops a nonzero value in the vicinity of the Maxwell value of $z = z_c$, growing approximately as a power law for $z > z_c$, though we cannot rule out a first-order transition. In the stressed state our data is consistent with a second-order rigidity threshold at $z = z_p \approx 2.7 < 3.0$, though again, we cannot rule out a first-order transition. For all β, $\log(G/\beta)$ grows linearly with $\log(z - z_p)$, where the slope is around 2.7 for $\beta = 10^{-4}$, 10^{-2} and 10^{-1} and then decreases with β to a value around 1.1 at $\beta = 10$. The fact that the slope depends upon β is not surprising, since for large β, we expect the deformation to be dominated by (affine) stretching of the segments, the number of which linearly increases with z, leading to a slope of 1. At small β, response to shear occurs preferentially through bending rather than stretching modes, and G is more sensitive to changes in z , as reflected in the larger value of the slope. For the smallest values of β, G becomes approximately linear in β for all values of z, which again demonstrates that bending dominates the deformation, as is the case in glasses [21].

There are many examples of structures in which external stresses can remove floppy modes. Here we show that internal stresses can have a similar effect, reminiscent of tensegrity structures, in which rigidity can be achieved below the Maxwell threshold by stressed cables and compressed struts in carefully designed configurations [22]. In contrast to these configurations, our networks are *random*, and rigidity is a

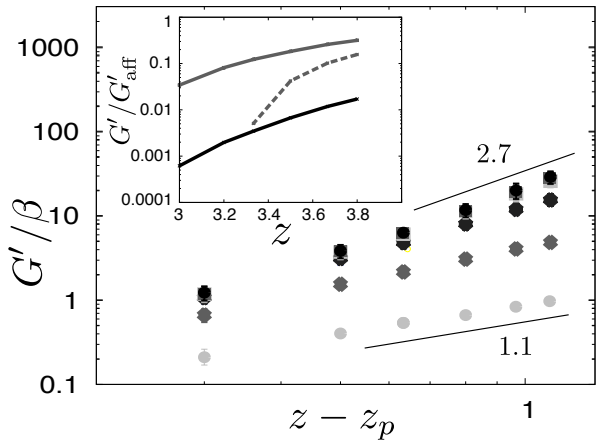

FIG. 2: Double logarithmic plot of G/β in networks with prestress as a function of $z-z_p$ for different values of β. Data points are from simulation, most error bars are smaller than the size of the symbols. The slope of the data points ranges from 2.7 upper, overlapping data points for $\beta = 0.0001$ and $\beta = 0.001$), 2.6 ($\beta = 0.01$), 2.1 ($\beta = 0.1$), 1.5 ($\beta = 1.0$) and 1.1 ($\beta = 10.0$, lower points). A value of $G = 1$ corresponds to an elastic modulus of ≈ 10 mPa for an actin network with a concentration f-actin of ≈ 0.05 mg/ml. Inset shows G/G_{aff} as a function of z, for $\beta = 1.0$ (upper curve) and $\beta = 0.01$ (lower curve). Dotted curve shows data from unstressed network, for $\beta = 1.0$.

consequence of competition between stretching and bending rather than between stretching and compression. If the network has a structure in which filaments can support self-stress, a modified Maxwell rule $N_0 = dN - N_c + S$, where S is the number of states of self-stress [23] or, equivalently, the number of redundant bonds [24], applies to the stressless state. Thus, even though global Maxwell counting would indicate the contrary, biopolymer networks with internal stresses may not have floppy modes and may support shear below the stressless Maxwell rigidity threshold.

Network geometry, co-ordination number, and spatial dimension are all important to the determination of macroscopic elastic response. Two-dimensional lattices with $z = 4$, such as the kagome lattice and the $L/l_c \to \infty$ limit of the Mikado lattice formed by the randomly depositing rods on a plane, are isostatic with respect to stretch, and they both exhibit affine response with non-zero shear and bulk moduli that are independent of β. The transition from non-affine bending-dominated to nearly affine stretching-dominated response observed in diluted Mikado lattices in Refs. [6, 7, 25] is thus not surprising. Three-dimensional systems with $z = 4$ are sub-isostatic with respect to stretch, and one might expect that bending forces are required for stabilization against shear. This is indeed the case for the $z = 4$ diamond lattice, none of whose bond-angles are zero (i.e., all filaments are straight), whose shear modulus vanishes linearly with β [21]. On the other hand, a recently constructed $3d$ generalization of the kagome lattice consisting of infinitely long straight filaments with crosslink coordination of exactly four provides a counter example to this behavior [26]. Because all its filaments are straight it has a persistent triangular motif, all of its elastic moduli are nonzero when $\beta = 0$. As is the case in most biopolymer networks and in the diamond lattice, the filaments in our network are not straight, so we expect behavior closer to that of the diamond lattice than to that of the straight-filament $3d$ lattice with non-affine bending dominated response and a shear modulus that vanishes with β even in the limit $z \to 4$. Though our simulations do not reach sufficiently close to $z = 4$ to unambiguously determine behavior at $z = 4$, they provide strong evidence that this expectation is fulfilled. As the inset in Fig. 2 shows, it is highly improbable that the affine limit, $G/G_{\rm aff} = 1$, is reached for small β. Instead, we find that $G \propto \beta$ for the smallest values of β in Fig. 2, implying that $G/G_{\rm aff}$ vanishes with vanishing β.

We now turn to the mode structure of these networks. The density of states $D(\omega)$ and the inverse participation ratio [15],

$$P^{-1}(\omega) = \frac{\sum_{i=1}^{N} |e_{i\omega} \cdot e_{i\omega}|^2}{|\sum_{i=1}^{N} e_{i\omega} \cdot e_{i\omega}|^2}, \qquad (2)$$

which provides a measure of the degree of localization of the eigenmodes, are plotted in Fig. 3. In Eq. (2), $e_{i\omega}$ is the polarization vector of node i in the mode ω. The value for $P^{-1}(\omega)$ will be 1.0 if the mode displaces one node, 0.5 if the mode displaces two nodes, and it will be $1/N$ for the translational zero modes that are linear transformations of the whole network. The data in Fig. 3 are averaged over narrow bins of frequency. The reduced frequency ω corresponds to physical frequencies $\widetilde{\omega} \approx 10^6 \omega\ s^{-1}$ for actin ($l_p = 16\mu m$ and $l_c = 1\mu m$) and $\widetilde{\omega} \approx 10^5 \omega\ s^{-1}$ for fibrin bundles ($l_p = 33\mu m$ and $l_c = 2\mu m$, as analyzed in [27]). These frequencies will increase if the viscosity of the surrounding fluid is included.

Fig. 3a shows the density of states, $D(\omega)$ as a function of $\log \omega$ with logarithmic binning for $\beta = 0.0001, 0.01$, and 1.0 at $z = 3.33$. For $\beta = 0.01$ and $\beta = 0.0001$, there is a peak in $D(\omega)$ at $\omega \approx 2$ that corresponds to stretching modes. Its total area for $\beta = 0.0001$ is equal to the number of stretching constraints, $2N - N_F$ or equivalently to the number of non-vanishing modes at $\beta = 0$. With increasing z, the area under the right peak increases, as we would expect from the increase in the number of stretching constraints (data not shown). There is a second peak at smaller ω that moves to the left as β decreases. We verified that the total area under this peak is $N_b' = N_0 + N_b$, where N_0 is the number of zero modes of the unstressed network, and N_b is the number of bending constraints. Where possible, shear deformation will take place via these soft bending modes. As we have seen, $G \sim \beta$ for small β, which implies that this is indeed the case. Again, we average over narrow bins of frequency with fixed logarithmic width to obtain $P^{-1}(\log\ \omega)$, which is plotted in Fig. 3b for $\beta = 0.0001$. Interestingly, both bending and stretching modes can be localized and delocalized.

Figs. 3c and 3d plot $D(\omega)$ and $P^{-1}(\omega)$ for different values of z and $\beta = 1.0$. The broad distribution in P^{-1} reflects the randomness in our system. Clearly the number of soft, low-frequency modes increases with decreasing z, and these

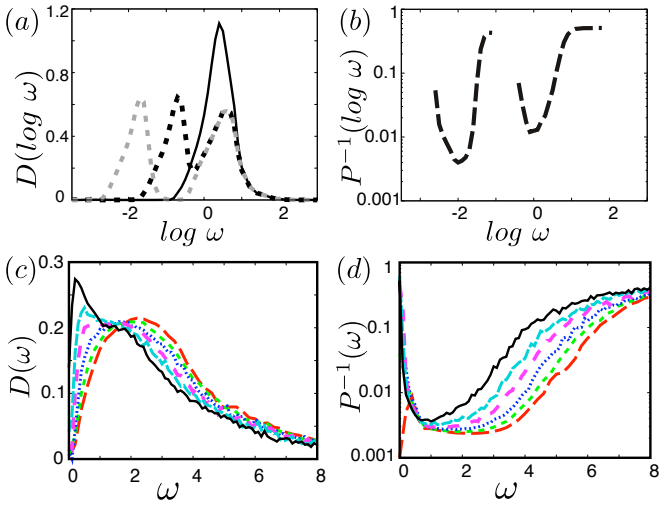

FIG. 3: a) The logarithm of the density of states, for $\beta = 1.0$ (solid curve), $\beta = 0.01$ (black dotted) and $\beta = 0.0001$ (grey dotted) for networks with $z = 3.33$. Note that the right peak of the latter two curves overlaps, and the left peak is shifted. b) The inverse participation ratio for $\beta = 0.0001$, again for $z = 3.33$. c) The density of states and d) the inverse participation ratio as a function of z. All data shown are for networks with $\beta = 1.0$ and (starting from the solid line) $z = 3.0$, $z = 3.2$, $z = 3.33$, $z = 3.5$,$z = 3.66$ and $z = 3.8$. Data shown are averaged over narrow bins of (the logarithm of) frequency.

modes are less extended. At low z, the filaments are less constrained in the networks, leading to an increase in soft deformation modes in the networks; in this limit, movement of a single segment will lead to a less extended deformation field. This is reflected in the increase of P^{-1} when decreasing z. We verified that the Debye scaling is approached and the frequency at which this scaling starts decreases for decreasing z. For $z = 3.0$ and $z = 3.2$ we do not find a peak in $D(\omega)$ at $\omega = 0$, which is consistent with the given analysis that internal stresses can remove floppy modes for $z < z_c$.

Our results show that networks with internal stress violate stressless Maxwell counting and exhibit rigidity and no floppy modes below the Maxwell isostatic threshold. This can be relevant for in vivo biopolymer networks, that might have large internal stresses which increase the stiffnesses of the cells [3]. As $\beta \to 0$, there is a clean separation between low-frequency bending modes and high-frequency stretching modes. As is the case in most *real life* biopolymer networks but contrary to that of most biopolymer networks studied analytically and in simulations, our networks consist of bent filaments. Our simulations show that it is highly improbable for this class of networks that the affine limit is reached for z approaching 4 at small β. Instead, the networks deform via low-frequency bending modes. Further investigation of this model, including a more thorough comparison with network glasses and a pebble-game analysis [24] to locate the critical point and to determine its order, would clearly be interesting.

It is a pleasure to acknowledge G. Barkema, F. MacKintosh and C. Storm for helpful discussions and E. van der Giessen and M. Thorpe for comments on an earlier version of this paper. EMH thanks P. Janmey and the University of Pennsylvania, where part of this work was done, for their generous hospitality. This work is supported in part by NSF-DMR-0520020 and NSF-DMR-0804900 (TCL), and by NIH-GM083272 (EMH)

[1] B. Alberts, A. Johnson, J. Lewis, M. Raff, K. Roberts, P. Walter, *Molecular Biology of the Cell*. 4th. Ed. (Garland, New York, 2008).
[2] E.L. Elson, *Annu. Rev. Biophys. Chem.* **17**, 397 (1988).
[3] K.E. Kasza, A.C. Rowat, J. Liu, T.E. Angelini, C.P. Brangwynne, G.H. Koenderink, D.W. Weitz, *Curr. Opinion Cell Biology* **19**, 101 (2007).
[4] P.A. Janmey et al., *Nature* (London) **345**, 89 (1997).
[5] F.C. MacKintosh, J. K as, and P.A. Janmey, *Phys. Rev. Lett.* **75** 4425 (1995); C. Storm et al., *Nature* (London) **435**, 191 (2005).
[6] D.A. Head, A.J. Levine, F.C. MacKintosh, *Physical Review E* **68**, 061907 (2003).
[7] J. Wilhelm, E. Frey, *Phys. Rev. Lett* **91**, 108103 (2003).
[8] E.M. Huisman et al., *Phys. Rev. Lett.* **99**, 208103 (2007).
[9] J. C. Phillips, *J. of Non-Cryst. Solids* **43**, 37 (1981).
[10] M. F. Thorpe, *J. of Non-Cryst. Solids* **57**, 355 (1983).
[11] M.F. Thorpe et al., *J. of Non-Cryst. Solids*, **266-269**, 859 (2000).
[12] W.H. Zachariasen, *J. Am. Chem. Soc.* **54**, 3842 (1932).
[13] A.J. Liu and S.R. Nagel, *Nature* **396**, 21 (1998).
[14] L.E. Silbert, A. J. Liu and S.R. Nagel, *Phys. Rev. Lett.* **95**, 098301 (2005).
[15] L.E. Silbert, A. J. Liu and S.R. Nagel, *Phys. Rev. E* **79**, 021308 (2009).
[16] C. Heussinger, E. Frey, *Phys. Rev. E* **75**, 011917 (2007).
[17] C. Heussinger, B. Schaefer, and E. Frey, *Phys. Rev. E* **76**, 031906 (2007).
[18] E.M. Huisman, C. Storm and G.T. Barkema, *Phys. Rev. E* **78**, 051801 (2008).
[19] N. Morone et al., *J. Cell Biol.* **174**, 851 (2006).
[20] J. C. Maxwell, *Philosophical Magazine* **27**, 294 (1865).
[21] H. He and M.F. Thorpe, *Phys. Rev. Lett.* **54**, 2107 (1985).
[22] D. E. Ingber, *Sci. Am. Jan.* (1998), p. 48; D. Stamenovic and D. E. Ingber, *Soft. Matt.* **5**, 1137 (2009).
[23] C. R. Calladine, *Int. J. Solids Structures* **14**, 161 (1977).
[24] D. J. Jacobs and M. F. Thorpe, *Phys. Rev. E* **53**, 3682 (1996); M. V. Chubynsky and M. F. Thorpe, *Phys. Rev. E* **76**, 041135 (2007).
[25] D.A. Head, F.C. MacKintosh, A.J. Levine *Phys. Rev. E* **68**, 025101 (2003).
[26] O. Stenull and T.C. Lubensky (network based upon kagome lattice); C. Broedersz and F. MacKintosh ('phantom' cubic lattic), private communication.
[27] I.K. Piechocka et al., *Biophys. J.* **98**, 10 (2010).